nature materials

ARTICLES

https://doi.org/10.1038/s41563-022-01296-0

Check for updates

Ultra-stable all-solid-state sodium metal batteries enabled by perfluoropolyether-based electrolytes

Xiaoen Wang[1]✉, Cheng Zhang[2,3]✉, Michal Sawczyk[4], Ju Sun[1], Qinghong Yuan[2,5], Fangfang Chen[1], Tiago C. Mendes[1], Patrick C. Howlett[1], Changkui Fu[2,3], Yiqing Wang[2], Xiao Tan[2], Debra J. Searles[2,6], Petr Král[4,7], Craig J. Hawker[8,9,10], Andrew K. Whittaker[2,3]✉ and Maria Forsyth[1]✉

Rechargeable batteries paired with sodium metal anodes are considered to be one of the most promising high-energy and low-cost energy-storage systems. However, the use of highly reactive sodium metal and the formation of sodium dendrites during battery operation have caused safety concerns, especially when highly flammable liquid electrolytes are used. Here we design and develop solvent-free solid polymer electrolytes (SPEs) based on a perfluoropolyether-terminated polyethylene oxide (PEO)-based block copolymer for safe and stable all-solid-state sodium metal batteries. Compared with traditional PEO SPEs, our results suggest that block copolymer design allows for the formation of self-assembled nanostructures leading to high storage modulus at elevated temperatures with the PEO domains providing transport channels even at high salt concentration (ethylene oxide/sodium = 8/2). Moreover, it is demonstrated that the incorporation of perfluoropolyether segments enhances the Na^+ transference number of the electrolyte to 0.46 at 80 °C and enables a stable solid electrolyte interface. The new SPE exhibits highly stable symmetric cell-cycling performance at high current density (0.5 mA cm^{-2} and 1.0 mAh cm^{-2}, up to 1,000 h). Finally, the assembled all-solid-state sodium metal batteries demonstrate outstanding capacity retention, long-term charge/discharge stability (Coulombic efficiency, 99.91%; >900 cycles with $Na_3V_2(PO_4)_3$ cathode) and good capability with high loading $NaFePO_4$ cathode (>1 mAh cm^{-2}).

Sodium ion batteries are recognized as attractive energy-storage devices for next-generation large-scale applications due to the high abundance and wide distribution of sodium resources.[1,2] In addition, benefiting from sodium's high theoretical specific capacity (1,165 mAh g^{-1}) and low redox potential (−2.714 V versus standard hydrogen electrode), the use of sodium metal as anodes further boosts overall battery capacity, enabling the next generation of low-cost, high-capacity batteries.[3,4] However, the development of sodium metal batteries faces various challenges.[5,6] For instance, the extensive use of highly flammable liquid carbonate electrolytes can lead to catastrophic hazards such as fire and explosions.

In contrast, the development of all-solid-state sodium metal batteries with the absence of any flammable liquid shows notable advantages for improving battery safety. Solvent-free polymer electrolytes are attractive due to their flexibility, suitable mechanical strength and high electrochemical stability.[7,8] Traditional poly(ethylene oxide) (PEO)-based solid polymer electrolytes (SPEs) show good sodium salt solubility due to the coordination between ether oxygen and Na^+; however, this interaction is relatively strong, which limits the Na^+ movements. As a result, low transference numbers (t_{Na+}), defined as the ratio of current carried by Na^+ to the total current carried by all mobile charges,[9,10] are obtained. Furthermore, due to the high reactivity of sodium metal, poor interfacial stability between PEO electrolytes and the sodium anode is another hindrance to achieving long-lifetime battery performance.[11]

The emergence of fluorinated electrolytes provides an effective method to stabilize metal anodes and improve cycling stability. In lithium batteries, for example, the fluorinated segments can provide a source to form LiF-rich components in solid-electrolyte-interphase (SEI), thus improving long-term battery stability.[12–15] Moreover, the use of fluorinated electrolytes improves high-voltage stability due to the ultra-high electrochemical stability of LiF,[16] which enables their application in high-voltage batteries.[12,17] Unfortunately, previous reports have tended to focus on the design of fluorinated liquid electrolyte and lithium battery applications.[18] Examination of SPEs with fluorinated components and their applications in sodium metal batteries has yet to be investigated.

In this work, a new class of fluorinated block copolymer is designed as a solid electrolyte for the development of highly stable, all-solid-state sodium metal batteries. We demonstrate that the introduction of perfluoropolyether (PFPE) domains into PEO-based electrolytes can effectively enhance the mechanical stability of polymer electrolytes due to the formation of self-assembled microstructures. Compared with non-fluorinated PEO electrolytes, PFPE-based SPEs improve Na^+ transport and increase Na^+ transference number due to the strong and specific PFPE–anion

[1]Institute for Frontier Materials (IFM), ARC Industry Training Transformation Centre for Future Energy Storage, storEnergy, Deakin University, Geelong, Victoria, Australia. [2]Australian Institute for Bioengineering and Nanotechnology, The University of Queensland, Brisbane, Queensland, Australia. [3]ARC Centre of Excellence in Convergent Bio-Nano Science and Technology, The University of Queensland, Brisbane, Queensland, Australia. [4]Department of Chemistry, University of Illinois at Chicago, Chicago, IL, USA. [5]State Key Laboratory of Precision Spectroscopy, School of Physics and Electronic Science, East China Normal University, Shanghai, P. R. China. [6]School of Chemistry and Molecular Biosciences and Centre for Theoretical and Computational Molecular Science, The University of Queensland, Brisbane, Queensland, Australia. [7]Departments of Physics, Pharmaceutical Sciences, and Chemical Engineering, University of Illinois at Chicago, Chicago, IL, USA. [8]Materials Research Laboratory, University of California Santa Barbara, CA, USA. [9]Materials Department, University of California Santa Barbara, CA, USA. [10]Department of Chemistry and Biochemistry, University of California Santa Barbara, CA, USA. ✉e-mail: xiaoen.wang@deakin.edu.au; c.zhang3@uq.edu.au; a.whittaker@uq.edu.au; maria.forsyth@deakin.edu.au

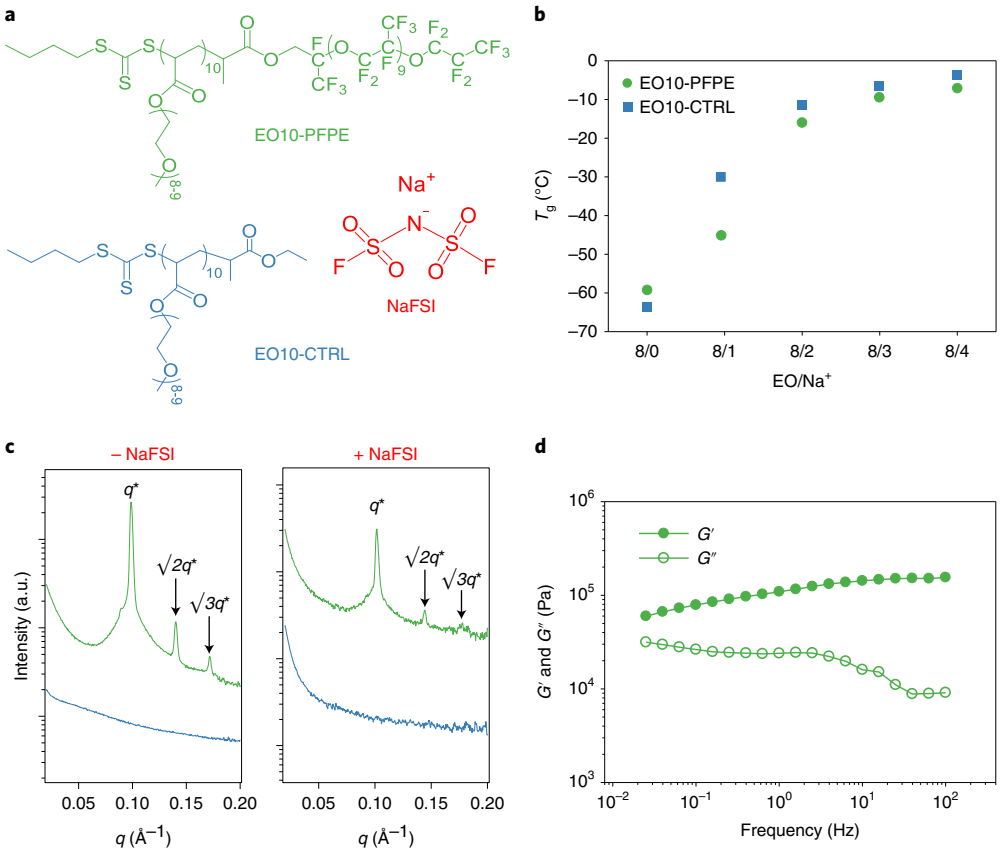


Fig. 1 | Chemical structures and physical properties of the polymer electrolytes. a, Chemical structures of poly(PEOA)$_{10}$-PFPE (EO10-PFPE), control homopolymer poly(PEOA)$_{10}$ (EO10-CTRL) and NaFSI salt. **b**, Dependence of glass transition temperature (T_g) of PEO on EO/Na ratios. **c**, SAXS profiles showing self-assembled structures of EO10-CTRL and EO10-PFPE with or without NaFSI. The X-axis is shown in the form of scattering vector q (q^* is the position of the most intense SAXS peak). **d**, Changes in storage modulus (G') and loss modulus (G'') of EO10-PFPE as a function of frequency at 80 °C.

interactions. In addition, the use of fluorinated moisture facilitates the formation of a stable SEI, leading to an outstanding plating/stripping stability (1,000 h) at 1.0 mAh cm^{-2}. Finally, all-solid-state sodium metal batteries based on fluorinated SPE composites show promising rate capability and long-term stability (>900 cycles with an average Coulombic efficiency of 99.91%). The study promises opportunities for the design of new fluorinated copolymers as highly stable solid polymer electrolytes for sodium battery applications.

Rational design and properties of PFPE electrolytes. We designed and investigated a class of fluorinated block copolymers with controlled morphology as a SPE to enhance mechanical integrity, interfacial stability and Na^+ transport. The copolymer consists of a PFPE segment as the fluorinated block and oligo(ethylene oxide) methyl ether acrylate (PEOA) as the soft block (EOm-PFPE, where m is the degree of polymerization of PEOA; see Methods and Supplementary Table 1 for details).[19–23] Fig. 1a illustrates the chemical structures of PFPE polymer (EO10-PFPE) and control polymer (EO10-CTRL). In this strategy, the dissociated Na^+ ions in the PEO domain undergo efficient transport with the assistance of ether oxygen side chain relaxation, while the phase separation between PEO and PFPE blocks maintains mechanical integrity. The fluorinated segments are also designed to stabilize the sodium metal in this study, through the formation of stable fluorinated compounds in the SEI layer.[24]

The interactions between polymers and alkali metal ions play a crucial role in the determination of polymer electrolyte properties and battery performance.[25–27] Investigation of the thermal behaviour, that is, the glass transition temperature (T_g), can help to understand such interactions in different electrolyte systems.[28] For example, differential scanning calorimetry measurements of neat EO10-PFPE copolymers show a T_g at −59.3 °C and an endothermic melting peak (T_m) located between −20 and 20 °C (Supplementary Figs. 1 and 2), associated with the glass-to-rubber relaxation and melting of the PEO domains, respectively. The glass transition and melt characteristics are well maintained in all PFPE-containing block polymers with different degrees of polymerization of PEOA. After adding NaFSI salt, the melting peak of PFPE polymers completely disappears (Supplementary Fig. 1). Another notable change is that, due to the strong coordination between ether oxygen and Na^+ ions, the addition of NaFSI (EO/Na = 8/1) increases the T_g of the PEO segments dramatically from approximately −60 °C to above −40 °C for all four EOm-PFPE copolymers (m = 5, 10, 20, 40) (Supplementary Fig. 2). Such changes are highly dependent on the salt concentration (that is, EO/Na; Fig. 1b, Supplementary Fig. 3 and Supplementary Table 2).

Interestingly, the introduction of the PFPE blocks enhances the relaxation of the PEO domain due to the formation of self-assembled body-centred cubic nanostructures (Fig. 1c). Compared with EO10-CTRL electrolyte, the EO10-PFPE with the same EO/Na^+ ratio shows a lower T_g when NaFSI is added (Fig. 1b). We ascribe the relatively lower T_g to the confinement effects on EO–Na^+ complex dynamics, which is in good agreement with previously reported hybrid electrolyte systems.[29,30]

The self-assembled body-centred cubic structures of EO10-PFPE electrolyte can be maintained at high temperatures with an order–disorder transition temperature (T_{ODT}) at 100 °C (Supplementary Fig. 4). Figure 1d shows the frequency sweep storage (G') and loss

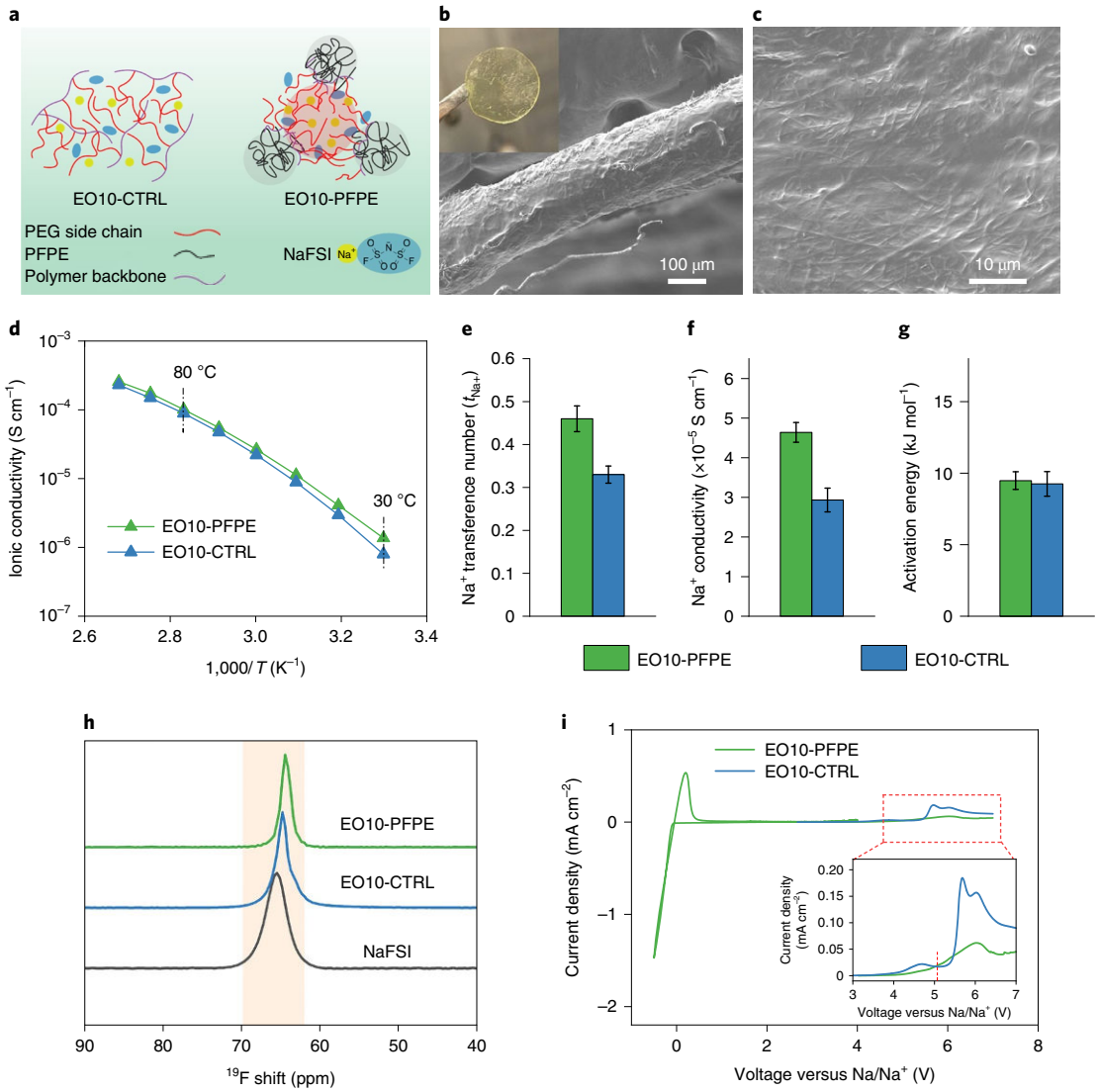
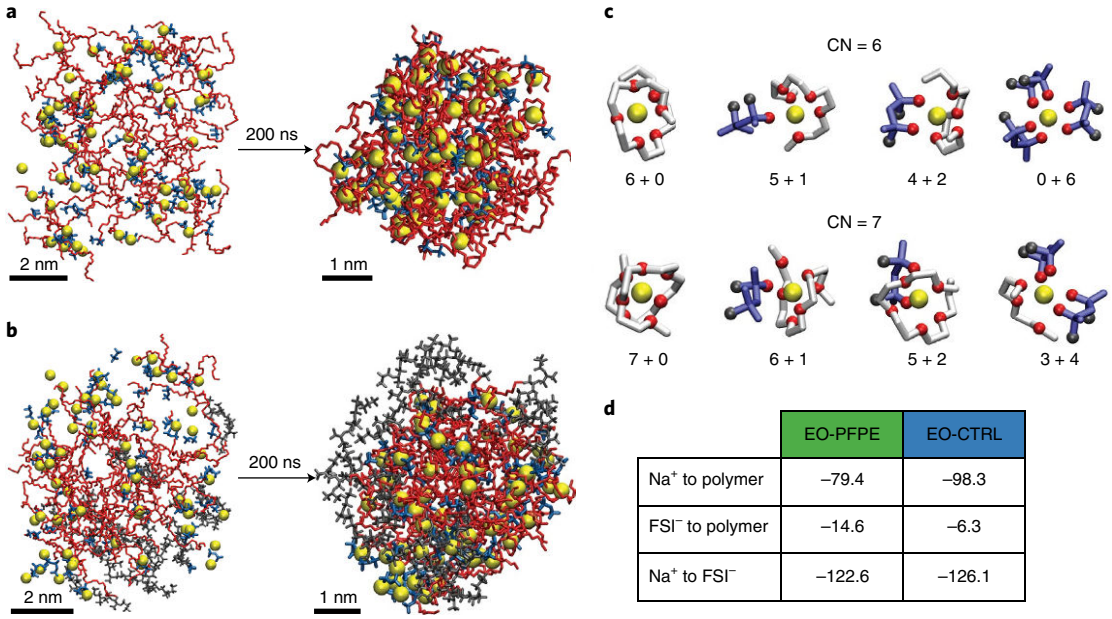


Fig. 2 | Morphology and electrochemical properties of the polymer electrolytes. a, Schematic illustration of proposed microstructures for EO10-CTRL and EO10-PFPE electrolytes. **b**,**c**, Cross-sectional (**b**) and surface (**c**) SEM images of EO10-PFPE composite SPE. Inset in **b**: photograph of a free-standing membrane. **d**, Conductivity comparison of EO10-PFPE and EO10-CTRL composite electrolytes. **e**–**g**, Comparison of Na^+ transference number (t_{Na+}) (**e**), Na^+ conductivity (**f**) and activation energy (E_a) (**g**) of EO10-PFPE and EO10-CTRL electrolytes at 80 °C. **h**, ^{19}F NMR spectra of EO10-PFPE, EO10-CTRL electrolytes and NaFSI salt. **i**, Cyclic voltammetry and linear sweep voltammetry profiles of EO10-PFPE composite SPE. The vertical red dashed line in inset represents the oxidation current intersection of two electrolytes. Scanning rate, 1 mV s^{-1} at 80 °C.

modulus (G'') of EO10-PFPE electrolytes at 80 °C. G' is distinctly greater than G'' over the full frequency window (10^{-2}–10^{2} Hz), implying a solid-like behaviour of the EO10-PFPE electrolyte. In addition, the storage modulus G' is closer to the loss modulus G'' at lower frequencies, indicating the soft behaviour of the electrolyte, potentially allowing the PFPE electrolyte to adapt and achieve good contact with the electrodes.[31] The self-assembly process is a thermodynamically or kinetically controlled process that is driven by the minimization of free energy in the system.[32–35] Such self-assembled nanostructures provide three-dimensional interconnected ionic transport channels and superior mechanical integrity, which are highly desirable for all solid battery devices and applications over a wide temperature range.[36]

Structures, interactions and electrochemical properties. Schematic illustrations of EO10-CTRL and EO10-PFPE electrolyte nanostructures are shown in Fig. 2a. Compared with the liquid-like EO10-CTRL electrolyte (Supplementary Fig. 5), the introduction of the PFPE block leads to the formation of a solid-state material with phase-separated PFPE-rich and PEO-NaFSI-rich domains. Incorporation of poly(vinylidene fluoride) (PVDF) electrospun fibres (Fig. 4a) results in a free-standing electrolyte membrane ~100 μm thick (Fig. 2b, inset). The scanning electron microscopy (SEM) images in Fig. 2b,c confirm that the pores of the PVDF matrix are completely filled with EO10-PFPE electrolyte, leading to a flexible, solvent-free SPE that is highly desirable for solid-state battery devices. By contrast, the EO10-CTRL composite is a soft and non-free-standing membrane which deforms easily, even in the absence of external force (Supplementary Fig. 6).

As shown in Fig. 2d, the conductivity of EO10-PFPE SPE is increased compared with that of the EO10-CTRL electrolyte over the whole temperature range, with the conductivity of EO10-PFPE reaching 1.0×10^{-4} S cm^{-1} at 80 °C. Given that the conductivity reported here is the apparent conductivity and the volume fraction of PEO phase is less than 100% (~85%; Supplementary Table 1), we expect that the true conductivity of the PEO-rich phase



d

	EO-PFPE	EO-CTRL
Na^+ to polymer	−79.4	−98.3
FSI^- to polymer	−14.6	−6.3
Na^+ to FSI^-	−122.6	−126.1

Fig. 3 | Molecular-level interactions between polymer electrolytes and NaFSI. a,**b**, Molecular dynamics simulations of EO-CTRL (**a**) and EO-PFPE (**b**) polymer electrolyte. The EO/Na^+ ratio is equal to 8/1. Na^+, yellow spheres; FSI^-, blue; EO chains, red; fluorinated fragment of the polymer, grey. **c**, Competitive Na^+ complexation motifs observed in the simulations for coordination numbers (CN) of six and seven. Red spheres, oxygen bound to sodium; black spheres, fluorine; white, EO backbone; purple, FSI^-. **d**, The calculated binding energies in kcal mol^{-1} of Na^+ to polymer, FSI^- to polymer and Na^+ to FSI^- for the last 1 ns of 200 ns simulation, normalized per 1 mole of ion. Note the binding energies do not include repulsion forces.

in EO10-PFPE is much higher than the conductivity reported in Fig. 2d (see Supplementary Fig. 7 for normalized conductivity). This enhanced conductivity could originate from the relatively low T_g (Fig. 1b) which facilitates the ion transport.[29] Another benefit of introducing PFPE into the polymer backbone is seen by the increased Na^+ transference number (t_{Na+} = 0.46 and 0.33 for EO10-PFPE and EO10-CTRL at 80 °C, respectively; Fig. 2e). Therefore, the EO10-PFPE shows increased Na^+ conductivity (total conductivity × t_{Na+}) of 4.7×10^{-5} S cm^{-1}, 1.5 times higher than that of the EO10-CTRL electrolyte (Fig. 2f). The Vogel–Fulcher–Tamman fitting results in Fig. 2g indicate that there is no notable change in activation energy in these two electrolytes. The role of PFPE segments is highlighted by the NMR results in Fig. 2h. As one moves from NaFSI to EO10-CTRL-NaFSI to EO10-PFPE-NaFSI, an upfield shift in ^{19}F NMR resonance is observed which correlates with stronger ion solvation or an increase in ion pairing; that is, there are increased interactions between FSI anions and PFPE polymer due to the previously reported 'fluorous effect'.[14,17,37] This anion–polymer interaction limits FSI mobility and enhances t_{Na+}, which is in good agreement with previous studies reported by Balsara and co-workers.[37]

The cyclic voltammetry results shown in Fig. 2i confirm a reversible plating and stripping process and absence of distinct oxidation (<4.0 V) when the EO10-PFPE electrolyte is used. The electrochemical stability window of EO10-PFPE is approximately 4.5 V, sufficient for most sodium battery applications.[38] It is notable that compared with EO10-CTRL, the EO10-PFPE shows a much lower oxidation current until 5 V, indicative of superior oxidative stability under high-voltage conditions. We attribute this increased oxidation stability to the formation of PFPE-rich domains.[14] As suggested by Bao and co-workers,[14] the formation of PFPE-rich domains limits the contact of EO repeat units with the electrode surface and protects the electrolyte from further oxidation at high voltage.

Molecular dynamics simulations were then performed to further understand the interactions between NaFSI and the polymer matrix (Supplementary Figs. 8–11). Fig 3a,b shows the different structures formed after 200 ns simulation time with the hydrophobic fluorinated chains closely packed at the surface, whereas the core of the assembly is composed of an ion-rich phase. For the EO-CTRL electrolyte, sodium ions are evenly distributed throughout the entire polymer matrix, forming EO–Na^+ complexes, whereas a distinct phase separation is observed in the EO-PFPE electrolyte (Supplementary Fig. 11). It can also be observed that sodium ions primarily locate in the PEO-rich phase, forming EO–Na^+ complexes, which explains the high dependence of T_g on NaFSI concentrations shown in the differential scanning calorimetry results in Fig. 1b. Furthermore, the molecular dynamics simulations revealed slightly different Na^+ binding patterns to EO-CTRL and EO-PFPE (Supplementary Figs. 12–14). We found that nearly all sodium cations were coordinated by six or seven oxygen atoms; however, the EO:FSI^- ratios in the complexes varied. Figure 3c displays the major structures observed in the simulations for both polymers, and Supplementary Fig. 15 shows the contribution of all $Na[(O_{EO})_x(O_{FSI})_y]$ combinations, where $x,y = 0–7$. The average coordination number of Na^+ (coordination number $= x + y$) ranged between ~6.3 (EO-PFPE) and ~6.7 (EO-CTRL), which indicates stronger binding of sodium to EO-CTRL than the latter, whereas the Na^+/FSI^- ratio was nearly identical for both polymers (Supplementary Fig. 13).

Figure 3d compares the binding energies between NaFSI and different components within the electrolytes (also seen in Supplementary Fig. 17). Compared with EO-CTRL, there is evidence of weakened interactions between EO-PFPE polymer chains and Na^+ (−79.4 kcal mol^{-1} versus −98.3 kcal mol^{-1}) with the binding energy between EO-PFPE and FSI^- doubled. This suggests that the addition of PFPE moieties into a PEO matrix will help 'release' more Na^+ while restricting the mobility of FSI anions, leading to increased t_{Na+} (Fig. 2e).[39] Another benefit of using PFPE blocks is the decrease in association energy between Na^+ and FSI^-. This could be rationalized by the additional FSI–polymer interactions, which lower the binding energy between sodium and FSI ions. In addition,

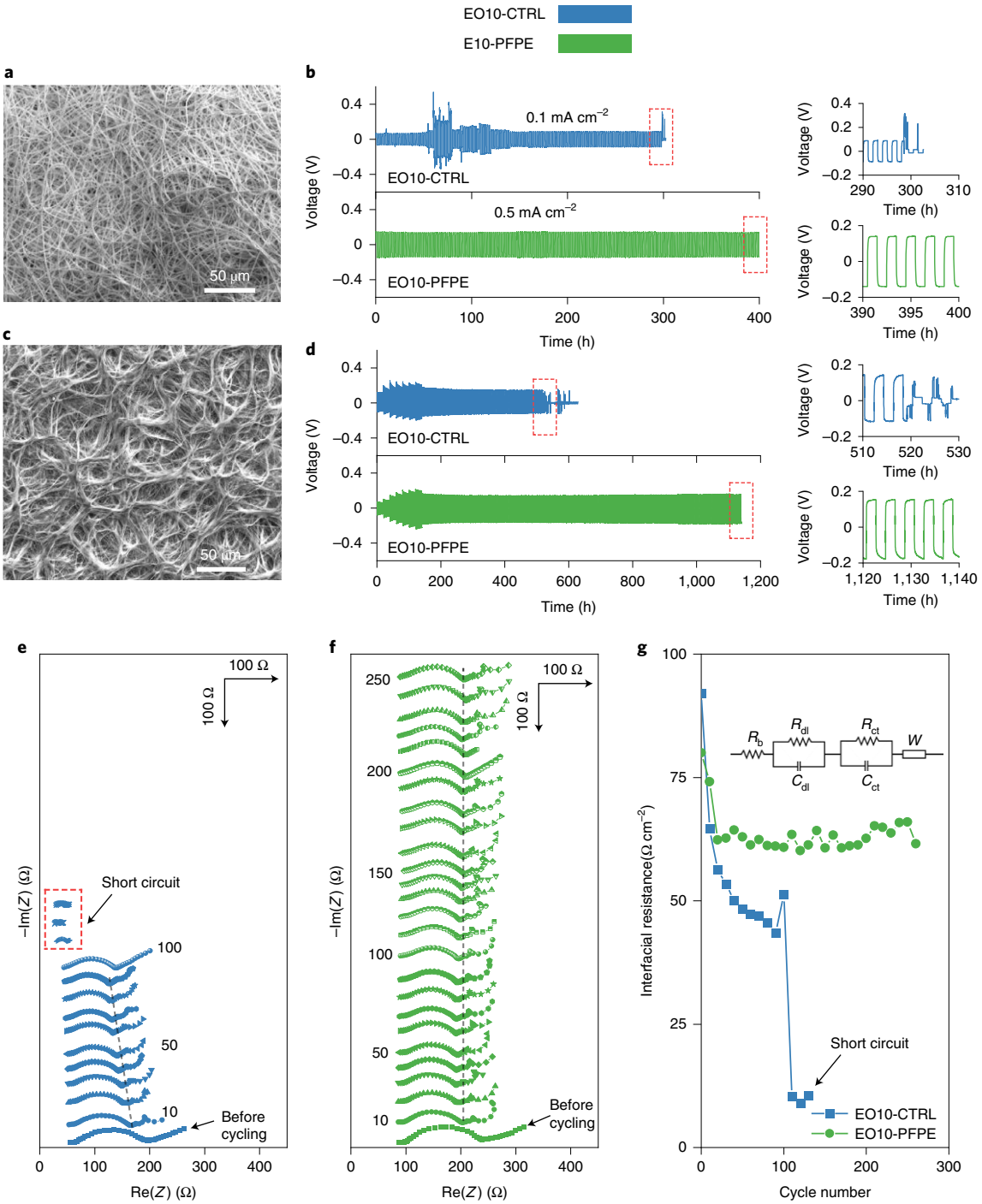


Fig. 4 | Na/Na plating/stripping performance. a, SEM image of PVDF electrospun nanofibres. **b**, Plating/stripping performance with composite electrolytes based on PVDF nanofibre separator. **c**, SEM image of the commercial Solupor separator. **d**, Plating/stripping performance with composite electrolytes based on the commercial Solupor separator. **e**–**g**, EIS evolution (**e**,**f**) and extracted interfacial resistance (**g**) during long-term Na/Na cycling at 0.5 mA cm^{-2} (1.0 mAh cm^{-2}, after 140 h as shown in **d**). The dashed gray lines represent the trend of overall cell resistance change during cycling. Inset in **g**: equivalent circuit. R_b represents the electrolyte bulk resistance. R_{dl} and R_{ct}, related to the interface resistance, are SEI resistance and charge-transfer resistance, respectively. C_{dl} and C_{ct} are the capacities associated with R_{dl} and R_{ct}, respectively. W represents the Warburg element. All the cell tests are performed at 80 °C.

the changes of interactions and coordination environments in EO-PFPE electrolytes, as suggested by molecular dynamics simulation, explains well their relatively high Vogel–Fulcher–Tamman pre-exponential factors (Supplementary Table 3) given the fact that the pre-exponential factor is proportional to the charge carrier concentration in most electrolyte systems.[40,41]

Na/Na symmetric cell performance. Further symmetric Na/Na cell tests confirm that the EO10-PFPE/PVDF composite exhibits extremely stable sodium plating/stripping behaviour at a high current density of 0.5 mA cm^{-2} (0.5 mAh cm^{-2}) for 200 cycles without obvious voltage oscillation (Fig. 4b, green). In contrast, the EO10-CTRL electrolyte can only be cycled at a much lower current

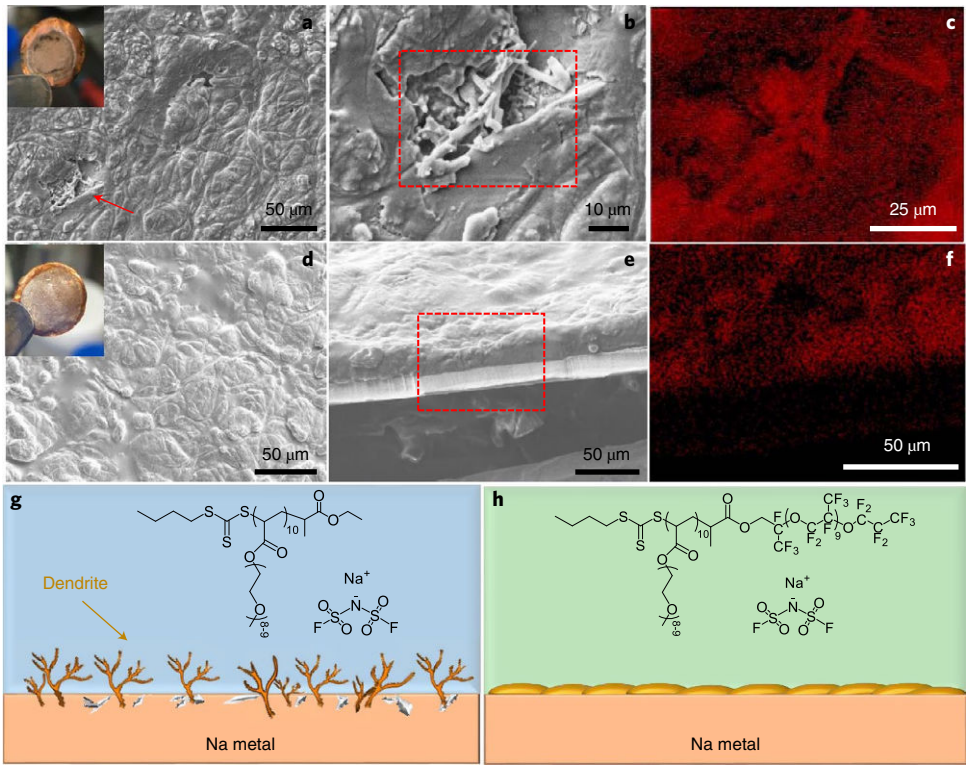


Fig. 5 | Morphologies of sodium metal deposition. a, Surface SEM image of deposited Na in a Na/Cu cell with EO10-CTRL electrolyte. **b**, The zoomed-in view of dendritic Na deposition as indicated by the red arrow in (**a**). **c**, The corresponding sodium EDS of the highlighted area in **b**. **d**,**e**, Surface SEM (**d**) and cross-section (**e**) images of deposited sodium in a Na/Cu cell with EO10-PFPE electrolyte. **f**, The corresponding sodium EDS of highlighted area in **e**. **g**,**h**, Schematic illustrations representing the potential SEI formation processes. Insets in **a** and **d**: digital photographs of deposited sodium on copper collectors with EO10-CTRL (**a**) and EO10-PFPE (**d**) electrolytes, respectively.

density of 0.1 mA cm^{-2} (0.1 mAh cm^{-2}). A severe voltage oscillation is observed, between 50 and 150 h in this case, suggesting the formation of an unstable SEI.[42] Further increase in the current density to 0.5 mA cm^{-2} leads to an immediately elevated overpotential and a final shorting failure of the symmetric cell in the control electrolyte (Fig. 4b, blue).

As discussed earlier, the EO10-CTRL electrolyte shows liquid-like behaviour and the resultant PVDF composite is a soft and non-free-standing film (Supplementary Figs. 5 and 6), which could affect the plating/stripping stability. To eliminate this mechanical limitation and further confirm the stability of EO10-PFPE, composite electrolytes using a commercial Solupor separator (Fig. 4c) were prepared (thickness, 80–90 μm) . These two symmetric cells both show the capability of cycling at different current densities from 0.05 to 0.6 mA cm^{-2} (1 h plating/1 h stripping; Fig. 4d). After 140 h, the cells were cycled at a constant current density of 0.5 mA cm^{-2}, but with a longer interval of 2 h (1.0 mAh cm^{-2}). Clearly, the EO10-CTRL/Solupor composite electrolyte exhibits a sudden short circuit after only 100 cycles, whereas the EO10-PFPE/Solupor composite electrolyte shows extremely stable cycling performance for 400 cycles (1,000 h) under harsh cycling conditions of 1.0 mAh cm^{-2} per cycle.

The superior stability with sodium metal achieved by using the EO10-PFPE electrolyte is further confirmed by comparison of impedance evolution. The overall cell resistance (highlighted in dashed grey line in Fig. 4e) of the Na/Na symmetric cell with EO10-CTRL/Solupor electrolyte continuously shifts to lower values followed by a dramatic decrease of overall resistance, indicative of cell failure due to short circuits. In sharp contrast, the symmetric cell assembled with EO10-PFPE/Solupor electrolyte demonstrates ultra-stable cell resistance during long-term cycling for over 1,000 h (Fig. 4f). The interfacial resistance comparison in Fig. 4g clearly demonstrates that a consistent value is maintained for the composite electrolyte with EO10-PFPE. Therefore, the ultra-stable plating/stripping performance, demonstrated by EO10-PFPE/PVDF and EO10-PFPE/Solupor, indicates the formation of a stable SEI between the PFPE-containing electrolyte and the sodium metal anode.

To further compare the changes in sodium metal morphology during the plating/stripping process, Na/Cu cells with different electrolytes were tested. It should be noted that the majority of Na/Cu plating/stripping experiments performed previously are based on liquid electrolytes, and the Coulombic efficiency (CE) of dry solid electrolytes has rarely been reported.[4] Nevertheless, the EO10-PFPE composite electrolyte shows promising stability, up to 400 cycles (average CE = 89.7%) with much lower overpotential, whereas the EO10-CTRL electrolytes failed after 80 cycles (average CE = 82.8%; Supplementary Fig. 18a–c). The lower overpotential (Supplementary Fig. 18d) confirms the efficient Na^+ transport of EO10-PFPE as indicated in Fig. 2f.

SEM images of the cycled sodium electrode surfaces reveal that uneven sodium deposits were formed on the copper current collector (indicated by arrows in Fig. 5a) when the EO10-CTRL electrolyte was used. The enlarged view shown in Fig. 5b and energy dispersive spectroscopy (EDS) mapping of sodium (Fig. 5c) further confirm the formation of dendritic sodium, suggesting the short-circuit failure mechanism. By contrast, a uniform deposition layer is maintained when EO10-PFPE was used (Fig. 5d). Thus, we can conclude that the incorporation of PFPE-moiety into PEO electrolyte greatly inhibits dendrite and void formation, resulting in a stable SEI on a sodium metal surface (Fig. 5g,h). It should be also mentioned that the sodium layer was densely deposited on the copper current

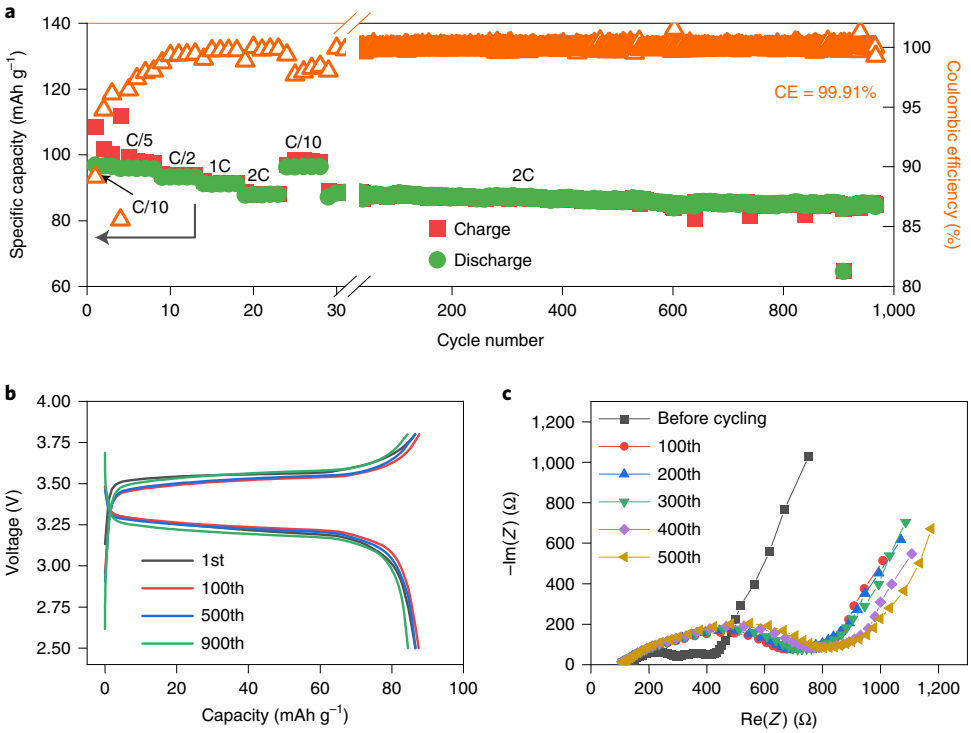


Fig. 6 | All-solid-state Na/NVP cell performance. a, Rate capability and long-term stability at ~0.2 mA cm^{-2} (2C). **b**,**c**, Charge/discharge profiles (**b**) and EIS evolution (**c**) during long-term cycling at 2C. Cut-off voltage, 2.5–3.8 V. All tests were performed at 80 °C. The N/P ratio is about 90/1 for the above test. A sodium metal battery with a much higher loading of 11.3 mg cm^{-2} and an N/P ratio of 7/1 is also reported in Supplementary Figs. 28 and 29.

collector (Fig. 5e,f). This morphology is beneficial to minimize side reactions and limit SEI growth, which strongly supports the stable plating/stripping performance shown in Fig. 4f.[38,43] The deposited sodium layer in Fig. 5f is surprisingly thick, which probably arises from the accumulation of sodium metal during long-term cycling and the relatively low CE.

Our design principle and the versatility of using fluorinated block copolymers is further proved by using a new block copolymer poly(oligo(ethylene glycol) methyl ether acrylate)-*b*-poly(trifluoroethyl acrylate) (EO10-TFEA; Supplementary Table 1). As shown in Supplementary Fig. 19, the Na/Na cell with EO10-TFEA electrolyte (EO/Na = 8/2) can also perform stable plating/stripping cycles at a high current density of 0.5 mA cm^{-2} for more than 550 h, highlighting the effectiveness of fluorinated polymers on SEI stabilization of sodium metal anode.

X-ray photoelectron spectroscopy results (Supplementary Figs. 20–25) confirm that SEI layers formed by EO10-PFPE and EO10-TFEA have a steadier trend of fluorine distribution during etching and more abundant fluorine (for example, 23.0% and 16.8% at 400 nm depth, respectively) than EO10-CTRL (9.8%), which benefits long-term battery cycling stability.[44–46] In addition, the excellent compatibility of EO10-PFPE electrolyte with a non-metal electrode such as hard carbon was also demonstrated (stable rate capability from 30 to 80 mA g^{-1} with the highest CE of 99.8%; Supplementary Fig. 26), which is highly desired for practical applications.

All-solid-state sodium metal battery performance. The electrochemical performance of the all-solid-state Na/NVP (NVP = $Na_3V_2(PO_4)_3$) batteries with EO10-PFPE/PVDF composite electrolyte was evaluated. As shown in Fig. 6a, the cell shows an initial discharge capacity of 96.8 mAh g^{-1}, and a relatively low initial CE of around 90% at C/10, which could be related to SEI formation.[47] When the current density was increased to C/5, C/2, 1C and 2C, the discharge capacities were 95.9, 93.1, 91.2 and 87.7 mAh g^{-1}, respectively. The cell promptly recovered to a capacity of 96.3 mAh g^{-1} when the C rate was returned to C/10, which indicates a superior capability of cycling at various C rates. More impressively, the all-solid-state sodium metal cell shows extremely long-term stability and high CE at 2C (~0.2 mA cm^{-2}). In particular, the discharge capacity only drops from 87.2 to 85.0 mAh g^{-1} after more than 940 cycles with a capacity retention of 97.5% (average capacity loss rate, 0.0026%) with an average CE higher than 99.9%. The superior cycling stability at high C rate is also confirmed by the charge/discharge profiles in Fig. 6b and it is apparent that the charge/discharge curves during the first 500 cycles essentially overlap. The recorded electrochemical impedance spectroscopy (EIS) spectra during 2C cycling measurements (Fig. 6c) suggest that the overall cell resistance increases after 100 cycles, which could result from increased interfacial resistance at high current density.[48] Encouragingly, the small resistance increase during the subsequent cycles highlights the capability of the EO10-PFPE/PVDF electrolyte to sustain high-rate cycling with high stability. Further evidence of the long-term stability of the electrolyte is also provided by additional cells cycled at a lower rate of C/2 shown in Supplementary Fig. 27.

To evaluate the capability of EO10-PEPE electrolyte for practical device applications, we prepared a cathode film with a high loading $NaFePO_4$ (NFP) cathode (11.3 mg cm^{-2}, with a theoretical areal capacity of 1.7 mAh cm^{-2}). After two initial cycles at C/20, the cell shows stable performance at C/10 (Supplementary Fig. 28a). In particular, the initial discharge capacity reaches 1.25 mAh cm^{-2}, and this capacity can still maintain at 1.1 mAh cm^{-2} after 50 cycles (80% capacity retention). Comparison of the charge–discharge profiles of cycles 1, 10, 30 and 50 (Supplementary Fig. 28b) demonstrates a negligible decay during the first 10 cycles and a small decay after the 30th cycle, demonstrating robustness and good compatibility with high loading cathodes when compared with EO10-CTRL (Supplementary Fig. 29). On the other hand, the cell

with EO10-CTRL electrolyte showed unstable charging behaviour after 550 h (Supplementary Fig. 29b,d), suggesting possible dendrite formation during sodium plating, as confirmed in Na/Na cycling tests (Fig. 4).

The outstanding performance of EO10-PFPE composite electrolyte demonstrated in the study is highlighted by comparison with previous studies based on other polymer or composite electrolytes (Supplementary Fig. 30 and Supplementary Table 4). It is clear that the EO10-PFPE composite electrolyte shows excellent capacity retention (97.5% after 940 cycles) and outstanding capacity output in sodium metal batteries and Na/Na cells.

Conclusions

We have demonstrated an ultra-stable all-solid-state sodium metal battery achieved using a PFPE-based block copolymer as the solid electrolyte. Our results confirm that incorporation of PFPE domains assists the formation of a self-assembled solid phase, leading to improved mechanical properties with enhanced storage modulus. Additionally, this phase-separated microstructure shows synergistic benefits for improving electrolyte performance, with molecular dynamics simulations confirming that the PFPE polymer has weakened interactions with sodium ions while enhancing interactions with FSI anions. As a consequence, both the Na^+ transference number and Na^+ conductivity are increased, which leads to the composite block copolymer electrolyte showing remarkable long-term cycling stability with a high capacity of 1.0 mAh cm^{-2} and excellent reversibility in long-term sodium plating/stripping tests. The assembled solid-state sodium metal batteries (with $Na_3V_2(PO_4)_3$ cathodes) demonstrate stable rate capability and outstanding charge/discharge reversibility (CE = 99.91%) at 2C (~0.2 mA cm^{-2}) after more than 900 cycles at an elevated temperature of 80 °C. Finally, we believe that fluorination is a general strategy to produce effective solid electrolytes by facilitating the formation of stable SEI.

Online content

Any methods, additional references, Nature Research reporting summaries, source data, extended data, supplementary information, acknowledgements, peer review information; details of author contributions and competing interests; and statements of data and code availability are available at https://doi.org/10.1038/s41563-022-01296-0.

Received: 26 March 2021; Accepted: 19 May 2022;
Published online: 4 July 2022

References

1. Zhao, Q. et al. Sodium-ion storage mechanism in triquinoxalinylene and a strategy for improving electrode stability. *Energy Fuels* **34**, 5099–5105 (2020).
2. Palomares, V. et al. Na-ion batteries, recent advances and present challenges to become low cost energy storage systems. *Energy Environ. Sci.* **5**, 5884–5901 (2012).
3. Cheng, X.-B., Zhang, R., Zhao, C.-Z. & Zhang, Q. Toward safe lithium metal anode in rechargeable batteries: a review. *Chem. Rev.* **117**, 10403–10473 (2017).
4. Zhao, Y., Adair, K. R. & Sun, X. Recent developments and insights into the understanding of Na metal anodes for Na-metal batteries. *Energy Environ. Sci.* **11**, 2673–2695 (2018).
5. Zhao, Q. et al. Tailored polyimide–graphene nanocomposite as negative electrode and reduced graphene oxide as positive electrode for flexible hybrid sodium-ion capacitors. *ACS Appl. Mater. Interfaces.* **10**, 43730–43739 (2018).
6. Ellis, B. L. & Nazar, L. F. Sodium and sodium-ion energy storage batteries. *Curr. Opin. Solid State Mater. Sci.* **16**, 168–177 (2012).
7. Forsyth, M., Porcarelli, L., Wang, X., Goujon, N. & Mecerreyes, D. Innovative electrolytes based on ionic liquids and polymers for next-generation solid-state batteries. *Acc. Chem. Res.* **52**, 686–694 (2019).
8. Wang, X. et al. Toward high-energy-density lithium metal batteries: opportunities and challenges for solid organic electrolytes. *Adv. Mater.* **32**, 1905219 (2020).
9. Mindemark, J., Lacey, M. J., Bowden, T. & Brandell, D. Beyond PEO—alternative host materials for Li^+-conducting solid polymer electrolytes. *Prog. Polym. Sci.* **81**, 114–143 (2018).
10. Rollo-Walker, G., Malic, N., Wang, X., Chiefari, J. & Forsyth, M. Development and progression of polymer electrolytes for batteries: influence of structure and chemistry. *Polymers* **13**, 4127 (2021).
11. Liu, L. et al. In situ formation of a stable interface in solid-state batteries. *ACS Energy Lett.* **4**, 1650–1657 (2019).
12. Yu, Z. et al. Molecular design for electrolyte solvents enabling energy-dense and long-cycling lithium metal batteries. *Nat. Energy* **5**, 526–533 (2020).
13. Fan, X. et al. All-temperature batteries enabled by fluorinated electrolytes with non-polar solvents. *Nat. Energy* **4**, 882–890 (2019).
14. Amanchukwu, C. V. et al. A new class of ionically conducting fluorinated ether electrolytes with high electrochemical stability. *J. Am. Chem. Soc.* **142**, 7393–7403 (2020).
15. Suo, L. et al. Fluorine-donating electrolytes enable highly reversible 5-V-class Li metal batteries. *Proc. Natl Acad. Sci. USA* **115**, 1156 (2018).
16. Richards, W. D., Miara, L. J., Wang, Y., Kim, J. C. & Ceder, G. Interface stability in solid-state batteries. *Chem. Mater.* **28**, 266–273 (2016).
17. Olson, K. R. et al. Liquid perfluoropolyether electrolytes with enhanced ionic conductivity for lithium battery applications. *Polymer* **100**, 126–133 (2016).
18. Qiao, L., Judez, X., Rojo, T., Armand, M. & Zhang, H. Review—polymer electrolytes for sodium batteries. *J. Electrochem. Soc.* **167**, 070534 (2020).
19. Zhang, C. et al. Tuning of the aggregation behavior of fluorinated polymeric nanoparticles for improved therapeutic efficacy. *ACS Nano* **14**, 7425–7434 (2020).
20. Zhang, C. et al. Integrating fluorinated polymer and manganese-layered double hydroxide nanoparticles as pH-activated ^{19}F MRI agents for specific and sensitive detection of breast cancer. *Small* **15**, 1902309 (2019).
21. Tan, X. et al. Amphiphilic perfluoropolyether copolymers for the effective removal of polyfluoroalkyl substances from aqueous environments. *Macromolecules* **54**, 3447–3457 (2021).
22. Zhang, C. et al. Biological utility of fluorinated compounds: from materials design to molecular imaging, therapeutics and environmental remediation. *Chem. Rev.* **122**, 167–208 (2022).
23. Zhang, C. et al. PFPE-based polymeric ^{19}F MRI agents: a new class of contrast agents with outstanding sensitivity. *Macromolecules* **50**, 5953–5963 (2017).
24. Li, T., Zhang, X.-Q., Shi, P. & Zhang, Q. Fluorinated solid-electrolyte interphase in high-voltage lithium metal batteries. *Joule* **3**, 2647–2661 (2019).
25. Wang, X. et al. Poly(ionic liquid)s-in-salt electrolytes with co-coordination-assisted lithium-ion transport for safe batteries. *Joule* **3**, 2687–2702 (2019).
26. Girard, G. M. A. et al. Sustainable, dendrite free lithium-metal electrode cycling achieved with polymer composite electrolytes based on a poly(ionic liquid) host. *Batter. Supercaps* **2**, 229–239 (2019).
27. Wang, X. et al. Preparation and characterization of gel polymer electrolytes using poly(ionic liquids) and high lithium salt concentration ionic liquids. *J. Mater. Chem. A* **5**, 23844–23852 (2017).
28. Stolwijk, N. A. et al. Salt-concentration dependence of the glass transition temperature in PEO–NaI and PEO–LiTFSI polymer electrolytes. *Macromolecules* **46**, 8580–8588 (2013).
29. Kinsey, T., Glynn, K., Cosby, T., Iacob, C. & Sangoro, J. Ion dynamics of monomeric ionic liquids polymerized in situ within silica nanopores. *ACS Appl. Mater. Interfaces* **12**, 44325–44334 (2020).
30. Kipnusu, W. K., Elmahdy, M. M., Elsayed, M., Krause-Rehberg, R. & Kremer, F. Counterbalance between surface and confinement effects as studied for amino-terminated poly(propylene glycol) constraint in silica nanopores. *Macromolecules* **52**, 1864–1873 (2019).
31. Yu, Z. et al. A dynamic, electrolyte-blocking, and single-ion-conductive network for stable lithium-metal anodes. *Joule* **3**, 2761–2776 (2019).
32. Zhang, C. et al. Emergence of hexagonally close-packed spheres in linear block copolymer melts. *J. Am. Chem. Soc.* **143**, 14106–14114 (2021).
33. Barbon, S. M. et al. Architecture effects in complex spherical assemblies of $(AB)_n$-type block copolymers. *ACS Macro Lett.* **9**, 1745–1752 (2020).
34. Bates, M. W. et al. Synthesis and self-assembly of AB_n miktoarm star polymers. *ACS Macro Lett.* **9**, 396–403 (2020).
35. Zhang, C. et al. Rapid generation of block copolymer libraries using automated chromatographic separation. *J. Am. Chem. Soc.* **142**, 9843–9849 (2020).
36. Min, J., Barpuzary, D., Ham, H., Kang, G. C. & Park, M. J. Charged block copolymers: from fundamentals to electromechanical applications. *Acc. Chem. Res.* **54**, 4024–4035 (2021).
37. Wong, D. H. C. et al. Nonflammable perfluoropolyether-based electrolytes for lithium batteries. *Proc. Natl Acad. Sci. USA* **111**, 3327–3331 (2014).
38. Tian, Y. et al. Reactivity-guided interface design in Na metal solid-state batteries. *Joule* **3**, 1037–1050 (2019).
39. Cong, L. et al. Role of perfluoropolyether-based electrolytes in lithium metal batteries: implication for suppressed Al current collector corrosion and the stability of Li metal/electrolytes interfaces. *J. Power Sources* **380**, 115–125 (2018).

40. Zheng, Q., Ma, L., Khurana, R., Archer, L. A. & Coates, G. W. Structure–property study of cross-linked hydrocarbon/poly(ethylene oxide) electrolytes with superior conductivity and dendrite resistance. *Chem. Sci.* **7**, 6832–6838 (2016).
41. Arkhipova, E. A., Ivanov, A. S., Maslakov, K. I., Savilov, S. V. & Lunin, V. V. Effect of cation structure of tetraalkylammonium- and imidazolium-based ionic liquids on their conductivity. *Electrochim. Acta* **297**, 842–849 (2019).
42. Pathirana, T., Kerr, R., Forsyth, M. & Howlett, P. C. Electrochemical formation in super-concentrated phosphonium based ionic liquid electrolyte using symmetric Li-metal coin cells. *J. Electrochem. Soc.* **167**, 120526 (2020).
43. Xiang, Y. et al. Visualizing the growth process of sodium microstructures in sodium batteries by in-situ ^{23}Na MRI and NMR spectroscopy. *Nat. Nanotechnol.* **15**, 883–890 (2020).
44. Chen, J. et al. Electrolyte design for LiF-rich solid–electrolyte interfaces to enable high-performance microsized alloy anodes for batteries. *Nat. Energy* **5**, 386–397 (2020).
45. Wang, Q. et al. Stabilizing a sodium-metal battery with the synergy effects of a sodiophilic matrix and fluorine-rich interface. *J. Mater. Chem. A* **7**, 24857–24867 (2019).
46. Xu, M. et al. NaF-rich solid electrolyte interphase for dendrite-free sodium metal batteries. *Energy Storage Mater.* **44**, 477–486 (2022).
47. Xiao, Y., Hwang, J.-Y., Belharouak, I. & Sun, Y.-K. Na storage capability investigation of a carbon nanotube-encapsulated $Fe_{1-x}S$ composite. *ACS Energy Lett.* **2**, 364–372 (2017).
48. Zhang, J.-N. et al. Dynamic evolution of cathode electrolyte interphase (CEI) on high voltage $LiCoO_2$ cathode and its interaction with Li anode. *Energy Storage Mater.* **14**, 1–7 (2018).

Publisher's note Springer Nature remains neutral with regard to jurisdictional claims in published maps and institutional affiliations.

© The Author(s), under exclusive licence to Springer Nature Limited 2022

Methods

Synthesis of EO-CTRL, EO-PFPE and EO10-TFEA polymers. Synthesis of the three polymers was performed according to our previously reported methods.[23] In a typical experiment for preparing EO10-PFPE, PFPE macro-reversible addition-fragmentation chain-trasfer (RAFT) agent (187 mg, 0.11 mmol), PEOA (770 mg, 1.6 mmol) and AIBN (3.28 mg, 0.020 mmol) were dissolved in trifluorotoluene (2 ml) and sealed in a 10 ml flask fitted with a magnetic stirrer bar. The solution was then deoxygenated by purging thoroughly with nitrogen for 15 min, heated to 65 °C in an oil bath, and allowed to react for ~4 h with conversion at ~70%. Upon completing the reaction, the solution was precipitated into hexane three times. The precipitate was then dried in a vacuum oven at 60 °C for 12 h, yielding a yellow viscous solid. Polymers with a range of PFPE compositions were prepared under identical conditions apart from differences in the initial feed amount between PEOA and PFPE macro-RAFT agent. The EO10-CTRL sample was prepared with the same procedure in the absence of PFPE macro-RAFT agent. EO10-TFEA was prepared by chain extension of EO10-CTRL using TFEA monomer aiming for a similar fluorine content to that of EO10-PFPE.

Polymer electrolyte preparation. The polymer electrolytes were prepared by a solvent casting method as described in previous literature.[25,49] In particular, PFPE polymer was dried at 50 °C under vacuum for 2 d and dissolved in dry acetonitrile together with dry NaFSI salt. For battery tests, composite electrolytes with incorporation of PVDF fibres were used, the composite electrolytes were prepared by casting prepared polymer solution with PVDF matrix according to our previous work.[25] The composites with Solupor separators were prepared the same way. The composites were finally dried under vacuum at least for 2 d to completely remove solvent and water residuals.

Characterizations. *NMR spectroscopy.* Solution-state ^{1}H and ^{19}F NMR spectra were recorded on a Bruker Avance 400 MHz (9.4 T) spectrometer in $CDCl_3$. Chemical shifts (δ) in ^{1}H NMR spectra are reported in ppm relative to the residual $CHCl_3$ (7.26 ppm). Solid-state NMR spectra were acquired on a Bruker 300 MHz spectrometer.

Small-angle X-ray scattering. Small-angle X-ray scattering (SAXS) measurements of EO10-CTRL and EO10-PFPE with NaFSI (EO/Na = 8/2, molar ratio) or without NaFSI were conducted at 80 °C using a custom-built SAXS diffractometer at the Materials Research Laboratory X-ray facility (University of California, Santa Barbara). For these experiments, 1.54 Å Cu Kα X-rays were generated using a Genix 50 W X-ray microsource (50 μm microfocus) equipped with FOX2D collimating multilayer optics (Xenocs) and high-efficiency scatterless single-crystal/metal hybrid slits. Samples were prepared using capillaries for SAXS experiments.

Ionic conductivity. The ionic conductivities of PFPE and control electrolytes (30–100 °C) were measured using EIS on a Solartron instrument (1 MHz–0.1 Hz with an amplitude of 10 mV). The samples were sealed in a home-made barrel cell in an argon-filled glovebox. The temperature was controlled via a Eurotherm 2204 controller, and the temperature was stabilized for 40 min before each test.

Coulombic efficiency. The Na/Cu cells were assembled in an argon-filled glovebox. The diameters of the copper and sodium discs were 10 and 8 mm, respectively. For each cycle, the experiments were done by plating 0.2 mAh cm^{-2} of sodium on the copper electrode (for 1 h with a current density of 0.2 mA cm^{-2}) followed by a stripping process at a current density of 0.1 mA cm^{-2} to a cut-off voltage of 1.0 V. All experiments were done at 80 °C.

Battery tests. All-solid-state sodium metal batteries comprising the $Na_3V_2(PO_4)_3$ (NVP) or NFP cathode were assembled in CR 2032 coin cells inside the argon-filled glovebox ($O_2 < 0.1$ ppm, $H_2O < 0.1$ ppm). The thickness of this sodium anode is 100 ± 10 μm. The sodium metal foil (Merck) was rolled and brushed, then cut into anode discs with a diameter of 8 mm (area, ~0.5 cm^2) as anode. Full cells were cycled in a VMP-3 potentiostat at 80 °C.

Data availability

All the data supporting the findings of this work are in the paper and Supplementary Information. Additional data are available from the corresponding authors upon reasonable request. Source data are provided with this paper.

References

49. Wang, X. et al. Poly(ionic liquid)s/electrospun nanofiber composite polymer electrolytes for high energy density and safe Li metal batteries. *ACS Appl. Energy Mater.* **2**, 6237–6245 (2019).

Acknowledgements

The authors acknowledge the support of the Australia–India Strategic Research Fund (AISRF 48515) and the Australian Research Council for funding through the Industry Transformation Training Centre Scheme (IC180100049). The research reported here was partially supported by the National Science Foundation (NSF) through the Materials Research Science and Engineering Center at UC Santa Barbara, DMR-1720256 (IRG-2). A.K.W. and C.Z. acknowledge support from the Australian Research Council (CE140100036) and National Health and Medical Research Council for an Early Career Fellowship (APP1157440 to C.Z.). The authors acknowledge the use of the facilities and the assistance of Y. Hora at the Monash X-ray platform. The Australian National Fabrication Facility, Queensland Node, is also acknowledged for access to some items of equipment.

Author contributions

X.W., C.Z. and M.F. conceived the idea. C.Z. designed and characterized the PFPE block polymers. C.F., Y.W. and X.T. prepared the block copolymers. X.W. led the electrolyte design, electrolyte characterization and battery experiments. T.C.M. synthesized the NFP active materials and prepared the cathodes. J.S. conducted XPS and interpreted results with C.Z. and X.W. M.S., Q.Y., F.C., D.J.S. and P.K. performed simulations and interpreted results. X.W. and C.Z. prepared the draft manuscript. P.C.H., C.J.H., A.K.W. and M.F. contributed to data interpretation and manuscript editing.

Competing interests

The authors declare no competing interests.

Additional information

Supplementary information The online version contains supplementary material available at https://doi.org/10.1038/s41563-022-01296-0.

Correspondence and requests for materials should be addressed to Xiaoen Wang, Cheng Zhang, Andrew K. Whittaker or Maria Forsyth.

Peer review information *Nature Materials* thanks Shinichi Komaba and Ying Shirley Meng for their contribution to the peer review of this work.

Reprints and permissions information is available at www.nature.com/reprints.